Design and Analysis of an Equivalent Load Power-Stability Control Circuit for Cabled Underwater Information Networks

LEI WANG[1], XUEJUN ZHOU[1], AND ZHENG ZHANG[ID][2]
[1]College of Electronic Engineering, Naval University of Engineering, Wuhan 430033, China
[2]Unit 75842, Chinese People's Liberation Army, Guangzhou 510000, China

Corresponding author: Xuejun Zhou (xuejun-zhou@163.com)

ABSTRACT Cabled underwater information networks (CUINs) have evolved over the last decade to provide abundant power and broad bandwidth communication to enable marine science. To ensure reliable operation of the CUINs, the stability of the remote power supply system, a key component of underwater power facilities, is essential. To avoid instability and collapse of the power system caused by rapid changes in load, we propose an equivalent load power-stability control circuit suited for an underwater constant current power supply system. This circuit can change its own working state according to the size of the load and play a role in power compensation. In order to prove the feasibility of the converter design, the working state of the circuit under different load values was analyzed and the performance of circuit was verified through simulation and experiments. The results show that when the load resistance changes within a large range (including when the load has an open circuit or short circuit fault), the equivalent load is basically unchanged or changed within a very small range for the constant current source, causing the constant current source to maintain stable output voltage and output power. Thus, the influence of the branch line cable on the trunk line cable is reduced, and the reliability of the underwater constant current power supply system is improved. Furthermore, the equivalent load power-stability control circuit would facilitate live equipment replacement and maintenance for CUINs.

INDEX TERMS Cabled underwater information networks (CUINs), remote constant current power supply system, stability, equivalent load power-stability control.

I. INTRODUCTION

The 21st century is the century of the ocean. The ocean is rich in natural resources and one of the main factors affecting the global environment and climate change. Moreover, exploring the ecosystem of the deep ocean is the key to understand the development of human civilization [1]–[4]. Over the last several decades, oceans have been observed with traditional shipborne and airborne mobile platforms or explored by underwater vehicles [5], anchored buoy stations, and battery-powered equipment [6]. However, these are only lateral, partial, and temporary ways to explore and research the ocean, and it is currently impossible to realize a full-scale, comprehensive, and real-time high-resolution stereoscopic observation of the ocean from the seabed to the surface [4], [7], [8]. In order to explore and understand the ocean and promote the development of marine science, the marine science community has proposed a third platform for observing the ocean [9], [10], that is, cabled underwater information networks (CUINs).

CUINs have surmounted the two major difficulties of energy supply and information transmission in ocean observation, and have become the mainstream development direction of the marine environment monitoring network [6]. Observation and electrical equipment in the networks relies on a remote power supply system connected to shore-based power supply equipment to provide energy. The remote power supply system serves as the energy supply, and its performance determines whether the CUINs can operate normally 11]. At present, the mainstream international submarine cabled power supply technology uses direct current power supply, and there are two types, i.e., the constant

The associate editor coordinating the review of this manuscript and approving it for publication was Zhiyi Li[ID].

voltage system and the constant current system, each system having its own advantages and disadvantages. For constant voltage power supply systems, the power converter module is connected in parallel with the trunk cable, and the power can be easily distributed through a mesh network [12], as with the North East Pacific Time-Integrated Undersea Networked Experiments (NEPTUNE-Canada) [13], [14] and other operating systems [15], [16]. For constant current power supply systems, a high-frequency switching converter is needed to shunt the primary node current on the trunk cable, keep the current in the trunk cable constant, and provide a constant current for the secondary node [11], [17], as with Japan 's Dense Ocean Network for Earthquakes and Tsunamis (DONET) [18], [19]. A system with a constant current power supply mode is resistant to cable impedance and faults. In the event of a short-circuit fault, parts of the system can still continue operating, and the system does not require high-medium-low voltage conversion [20]. Furthermore, the constant current power supply mode has the advantages of modularization and standardization of the electric energy conversion modules [11]. Therefore, the constant current method is a better choice than constant voltage in scenarios where reliability is more important than other features such as efficiency or power delivery capacity [21].

CUINs rely on observation nodes to observe and transmit information. In the constant current power supply mode, the observation node is powered by the constant current remote power supply system, which generally includes two types of converters: constant current to constant current (CC/CC) and constant current to constant voltage (CC/CV). The CC/CC converters are responsible for shunting the trunk cable current. The CC/CV converters mainly convert constant current to constant voltage in order to provide energy for transmission and for controlling and monitoring equipment in the nodes [22]. Regardless of whether they are open-loop control or closed-loop control, the CC/CC converters and CC/CV converters in the nodes only perform electrical energy conversion and cannot stabilize the output power of the nodes. When the resistance of the electrical equipment in the nodes changes, especially rapidly, the output power of the node will be unstable, which will cause the power system to become unstable or even crash.

Without proper control, rapid changes in load can result in instability and even collapse of the power system, so each load point (or junction box where scientific equipment will be attached to the system) must be ''smart'' enough to keep load variations within tolerance bounds [23]. Therefore, it is important to design a load power-stability controller that can ensure stability of the power supply system.

Harris and Duennebier [23] found that the Hawaii Undersea Geo-Observatory (HUGO) delivered approximately 5 kW usable power at the junction box (JBX), which was regulated to 350 V by a shunt regulator at the JBX, dumping excess power into a resistor stack. Petitt *et al.* [24] proposed a JBX for the Hawaii-2 Observatory (H2O), which delivered a modest 400W, with inputs in series and outputs in parallel

converters and a shunt regulator. Howe *et al.* [25] designed eight converters for the Aloha Cabled Observatory (ACO) in North America, with 100-V input and a regulated 48-V output. Each converter provided 160 W and the power consumed by shunts was controlled by sensing the input voltage to the converter. Kasahara *et al.* [26] proposed a versatile eco-monitoring network which delivered 175-W power for scientific instruments via a cabled underwater system. Kawaguchi *et al.* [27] and Yokobiki *et al.* [28] proposed a power distribution control system used in a dense ocean-floor network detection system for earthquakes and tsunamis in Japan. This system received 500-W constant direct current power supplied by the terminal equipment and distributed 45-W secondary power output to a measurement instrument as needed. Moreover, this power distribution control system had a mechanism to balance the power consumption of science nodes constants to prevent the system from reaching an unstable power distribution status. Chen *et al.* designed a typical CC/CV converter that comprised a shunt regulator and a CC/CC module [29]. The CC/CC module was an output-unregulated converter and functioned by stepping down voltage or boosting the current of the delivery power. The shunt regulator comprised a controller and a balance load (BL, also known as a 'dummy load') [30]. By sampling the external load voltage, the controller adjusted the resistance of the BL to keep the total power consumed on the BL and external load at a constant level. Chen *et al.* [31] conceived a multi-module-stack CC/CV converter architecture with active soft bypass (ASB) technology and a priority-based power management strategy (PPMS). The goal was to solve the incompatibility of high stability, reliability, and relatively high efficiency presented by the previous CC/CV converter.

A review of the current literature shows that the realization of load-side power stabilization controllers suitable for underwater constant current remote power supply system usually requires linear regulators [23]–[25], [32] or controllers [29]–[31] to drive power compensation circuits. As output power changes at nodes in a power network, due to load change, power compensation circuits can make the circuit and load jointly equivalent to a stable load resistance. The working principle of the linear regulator is shown in Figure 1(a). Only when the external load resistance becomes larger does the linear regulator come into play to bear the excess power consumption and maintain input power stability throughout the circuit. When the external load is reduced, the linear regulator will not function to maintain stability of the input and output of the circuit. The working principle of the controller is shown in Figure 1(b). It can adjust the resistance of the parallel balanced load according to the change in external load resistance, thereby maintaining stability of input power. However, it requires a sampling and control circuit, which will undoubtedly increase the complexity of the circuit and reduce the robustness of the power supply system.

In this article, we describe a novel power compensation circuit which combines simplicity and reliability. Using the
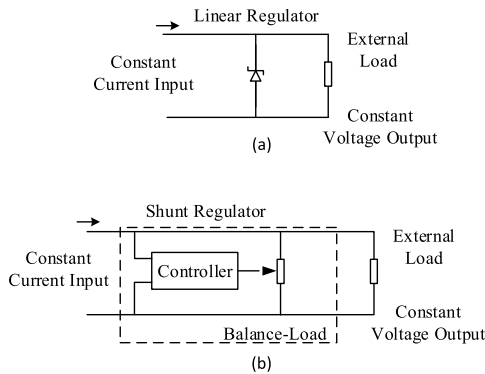
FIGURE 1. Schematic diagram of typical equivalent load power-stability control circuit in constant current power supply mode: (a) Diagram of equivalent load power-stability control circuit with linear regulator; (b) Diagram of equivalent load power-stability control circuit with controller.

interaction of the MOSFETs and the zener diodes, the circuit changes the working state of the MOSFETs according to the load, allowing power compensation. Through theoretical analysis, simulation, and experiment, the feasibility and stability of the circuit design was verified. The circuit proposed in this article can be connected in series between the constant current power supply and the load. When the resistance of the electrical equipment changes (including when the load has an open circuit or short circuit fault), the load and the control circuit on the observation nodes of the CUINs can be jointly equivalent to a stable load, which reduces the influence of the branch line cable on the trunk line cable and ensures that the output power of the supply network is stable. This not only improves the stability and reliability of the power supply system, but also facilitates standardization of the underwater information network.
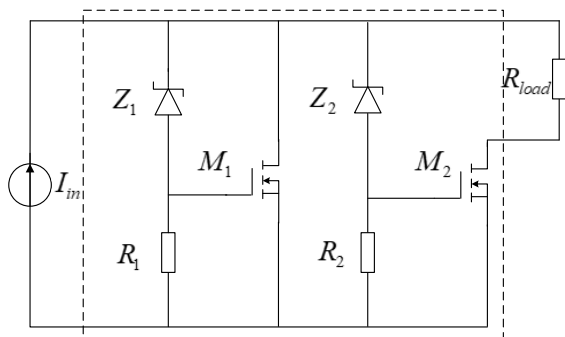

FIGURE 2. Schematic diagram of the equivalent load power-stability control circuit.

II. TOPOLOGY STRUCTURE OF THE EQUIVALENT LOAD POWER-STABILITY CONTROL CIRCUIT AND ANALYSIS OF THE WORKING CHARACTERISTICS OF MOSFETS

The basic structure of the equivalent load power-stability control circuit suited for the constant current power supply system proposed in this article is shown in Figure 2. In the figure, I_{in} is a constant current source, Z_1 and Z_2 are zener diodes, M_1 and M_2 are N-channel enhancement MOSFETs with the same performance, R_1 and R_2 are the current-limiting

resistors, and R_{load} is the load resistance. The design function of this circuit is that, regardless of the value of the load, the output power of the constant current source is basically stable at a certain value. The control principle of the circuit is that, because the energy supply is a constant current source, so long as it has a stable output voltage, the current source will also have a stable output power. In order to achieve a stable output voltage, regardless of the load resistance value, the control circuit and the load should be jointly equivalent to a fixed and stable resistance value. This means that other components of the circuit must bear the excess power generated by the load change.
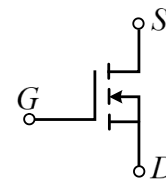

FIGURE 3. Structural diagram of N-channel enhancement MOSFET.

Before analyzing the operating characteristics of the circuit, we first introduce the characteristics of the main components: N-channel enhancement MOSFETs [33]. Figure 3 shows a structural diagram of an N-channel enhancement MOSFET, where S is the source, G is the gate, and D is the drain.

The working states of an N-channel enhancement MOSFET include an unsaturation region and a saturation region, and the difference between these regions is determined by the voltage between the drain and the source. The dividing line between the unsaturation and saturation regions is;

$$V_{DSC} = V_{GS} - V_T \qquad (1)$$

where, V_{GS} is the voltage between the gate and the source, V_T is the turn-on voltage of the MOSFET, and when $V_{GS} > V_T$, the MOSFET is turned on. When $V_{DS} \geq V_{DSC}$, the MOSFET is working in the saturation region, while when $V_{DS} < V_{DSC}$, the MOSFET is working in the unsaturation region. In the unsaturation region, the relationship between the drain-source current I_{DS}, the gate-source voltage V_{GS}, and the drain-source voltage V_{DS} of the MOSFET is;

$$I_{DS} = B_o[2(V_{GS} - V_T)V_{DS} - V_{DS}^2] \qquad (2)$$

where, B_o is only related to the properties of the MOSFET and does not change with the external voltage V_{GS} and V_{DS}.

In the saturation region, the drain-source current I_{DS} of the MOSFET is approximately;

$$I_{DS} = B_o(V_{GS} - V_T)^2 \qquad (3)$$

According to (3), the I_{DS} is only relevant to V_{GS} in the saturation region. If we consider the influence of V_{DS} on the length of the MOSFET drain-source conductive channel, when V_{DS} increases, I_{DS} will also increase slightly, which can be expressed as follows, where $0 < \lambda \ll 1$ [33];

$$I_{DS} = B_o(V_{GS} - V_T)^2(1 + \lambda V_{DS}) \qquad (4)$$

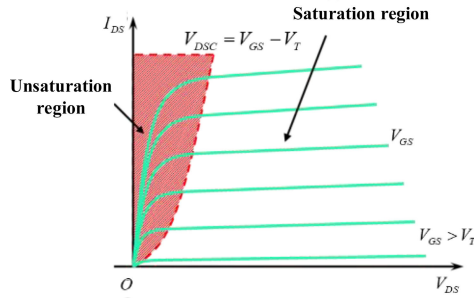The output characteristics of the unsaturation and saturation regions of the MOSFET are shown in Figure 4.

FIGURE 4. Output characteristic curves of an N-channel enhancement MOSFET.

III. ANALYSIS OF THE WORKING PRINCIPLES OF THE EQUIVALENT LOAD POWER-STABILITY CONTROL CIRCUIT

Because the power supply in Figure 1 is a constant current source, when $0 \leq R_{load} < \infty$, if the output voltage of the constant current source stabilized near a certain value, the output power of the constant current source stabilized at a certain value. Therefore, in the subsequent analysis, only the change of the output voltage of the constant current source will be considered. For convenience, it is assumed that the values of the two virtual resistances R_{E1} and R_{E2} are;

$$\begin{cases} R_{E2} = \dfrac{V_{Z2} + V_T}{I_{in}} \\ R_{E1} = \dfrac{V_{Z1} + V_T}{I_{in}} \end{cases} \qquad (5)$$

where, V_{Z1} and V_{Z2} are the stabilizing voltage value of Z_1 and Z_2, and $V_{Z1} > V_{Z2}$, i.e. $R_{E1} > R_{E2}$, V_T is the turn-on voltage of M_1 and M_2, and I_{in} is the output current of the constant current source. The working principle of the equivalent load power-stability control circuit is analyzed in three cases with different loads. The current shunt of the zener diode branch is ignored in the analysis.

A. $R_{load} \in [0, R_{E2}]$

Since the power supply in Figure 1 is a constant current source, the output voltage V_{in} of the constant current source is zero at the initial moment and there is no current in the circuit. Then the voltage V_{in} rises, and when it rises to $V_{in} = V_{Z2} + V_T$, MOSFET M_2 begins to turn on. At this time V_{GS2}, which is the voltage between the gate and the source of M_2, is;

$$V_{GS2} = V_{in} - V_{Z2} \qquad (6)$$

When M_2 is turned on, the drain-source voltage V_{DS2} is;

$$V_{DS2} = V_{in} - I_{in}R_{load} \qquad (7)$$

Because of $R_{load} \leq R_{E2}$, combining (5) and (7), produces;

$$V_{DS2} \geq V_{GS2} - V_T \qquad (8)$$

Satisfying the condition of $V_{DS} \geq V_{GS} - V_T$, the MOSFET M_2 works in the saturation region, and the drain-source current I_{DS2} is determined by the voltage V_{GS2}. From (4), I_{DS2} is;

$$I_{DS2} = B_o(V_{GS2} - V_T)^2(1 + \lambda V_{DS2}) \qquad (9)$$

If $I_{DS2} < I_{in}$, the constant current source will increase the output voltage, and the voltage V_{GS2} will increase accordingly, and eventually I_{DS2} will continue to increase. When $I_{DS2} = I_{in}$, the voltage V_{in} and voltage V_{GS2} no longer increase, the circuit reaches a steady state. A small change of V_{GS2} in this steady state will cause a large change of I_{DS2}.

In this steady state, the load can be equivalent to be powered by a constant current source, and the load current is;

$$I_{load} = I_{in} \qquad (10)$$

From (6), it can be seen that the voltage change of V_{GS2} is equal to the change of V_{in}. The voltage V_{GS2} must satisfy (9) and $I_{DS2} = I_{in}$. V_T and B_0 are both fixed values which are only related to the properties of the MOSFETs. Therefore, the maximum V_{GS2} is obtained when V_{DS2} is the minimum, and the minimum V_{GS2} is obtained when V_{DS2} is the maximum.

From (7), V_{DS2} is the minimum when $R_{load} = R_{E2}$;

$$V_{DS2MIN} = V_{GS2} - V_T \qquad (11)$$

Substituting (11) into (9), V_{GS2MAX} can be obtained;

$$V_{GS2MAX} = \sqrt{\dfrac{I_{in}}{B_0[1 + \lambda(V_{GS2MAX} - V_T)]}} + V_T \qquad (12)$$

Similarly, from (7), V_{DS2} is the maximum when $R_{load} = 0$;

$$V_{DS2MAX} = V_{in} \qquad (13)$$

Substituting (13) into (9), V_{GS2MIN} can be obtained as;

$$V_{GS2MIN} = \sqrt{\dfrac{I_{in}}{B_0(1 + \lambda V_{in})}} + V_T \qquad (14)$$

According to (12) and (14), the voltage variation of V_{GS2} is;

$$\Delta V_{GS2} = \sqrt{\dfrac{I_{in}}{B_0}}\left(\dfrac{1}{\sqrt{1 + \lambda(V_{GS2MAX} - V_T)}} - \dfrac{1}{\sqrt{1 + \lambda V_{in}}}\right)$$
$$< \sqrt{\dfrac{I_{in}}{B_0}}\left(1 - \dfrac{1}{\sqrt{1 + \lambda V_{in}}}\right) < \sqrt{\dfrac{I_{in}}{B_0}} \qquad (15)$$

Assuming that the output current of the constant current source is 1A and $B_0 \approx 1$, then $\Delta V_{GS2} < 1V$. $\Delta V_{GS2} = \Delta V_{in}$ can be determined from (6), therefore, when the load changes between 0 and R_{E2} (including a short-circuit fault of the load, i.e. $R_{load} = 0$), $\Delta V_{in} < 1V$. Even if $B_0 = 0.1$, ΔV_{in} is less than 3.3V.

From (9), when $I_{in} = I_{DS2} = 1A$ and $B_0 \approx 1$, $V_{GS2} \approx V_T$. So the output voltage of the constant current source in this steady state is,

$$V_{in} = V_{Z2} + V_{GS2} \approx V_{Z2} + V_T \qquad (16)$$

When $R_{load} \in [0, R_{E2}]$, for the constant current source, the equivalent load resistance R_{eq} of this control circuit and load is;

$$R_{eq} = R_{E2} \tag{17}$$

The power consumption borne by the M_2 is;

$$P_{M2} = V_{DS2}I_{in} = V_{in}I_{in} - I_{in}^2 R_{load} \tag{18}$$

Since $V_{in}I_{in}$ is approximately a fixed value, the smaller the load resistance is, the greater the power consumption P_{M2}. In extreme cases, when $R_{load} = 0$, the power consumption of M_2 is the largest and P_{M2MAX} is equal to the input power P_{in}. Larger power consumption causes the MOSFETs to heat up, and the increased temperature will reduce the service life of the MOSFETs. Therefore, in practice, the power consumption of MOSFETs should be reduced as much as possible.

B. $R_{load} \in (R_{E2}, R_{E1})$

From (5), when $R_{load} \in (R_{E2}, R_{E1})$, we can obtain the result is;

$$V_{Z2} + V_T < I_{in}R_{load} < V_{Z1} + V_T \tag{19}$$

It is not difficult to judge that M_1 is not yet turned on and that the output current of the constant current source is still flowing through M_2 at this time. Combining (5) and (7), the drain-source voltage V_{DS2} of M_2 satisfies;

$$V_{DS2} < V_{GS2} - V_T \tag{20}$$

V_{DS2} no longer meets the condition $V_{DS} \geq V_{GS} - V_T$, the MOSFET M_2 works in the unsaturation region, and I_{DS2} meets the following conditions;

$$I_{DS2} = B_o[2(V_{GS2} - V_T)V_{DS2} - V_{DS2}^2] = I_{in} \tag{21}$$

Assuming $I_{in} = 1A$ and $B_0 \approx 1$, according to (21), V_{DS2} is very small (usually less than 1V) and the voltage V_{DS2} is negligible compared with the load voltage, so the output voltage of the constant current source is;

$$V_{in} = I_{in}R_{load} + V_{DS2} \approx I_{in}R_{load} \tag{22}$$

When $R_{load} \in (R_{E2}, R_{E1})$, according to (19), the change of constant current source output voltage V_{in} is ($V_{Z2} + V_T$, $V_{Z1} + V_T$), so the change of V_{in} is;

$$\Delta V_{in} = V_{Z1} - V_{Z2} \tag{23}$$

When $R_{load} \in (R_{E2}, R_{E1})$, for the constant current source, the equivalent load resistance R_{eq} of this control circuit and load is;

$$R_{load} \in (R_{E2}, R_{E1}) \tag{24}$$

The power consumption of M_2 is $P_{M2} = V_{DS2}I_{in}$, and V_{DS2} is usually less than 1V. Assuming $I_{in} = 1A$, we can obtain $P_{M2} < 1W$.

C. $R_{load} \in [R_{E1}, \infty]$

When $R_{load} \in [R_{E1}, \infty]$, if M_1 is not turned on, there is a relationship of $I_{in}R_{load} \geq V_{Z1} + V_T$. So, the voltage of the current source should meet $V_{in} = I_{in}R_{load} + V_{DS2} > V_{Z1} + V_T$. Therefore, the gate-source voltage V_{GS1} of M_1 is;

$$V_{GS1} = V_{in} - V_{Z1} > V_T \tag{25}$$

Therefore, when $R_{load} \in [R_{E1}, \infty]$, MOSFET M_1 is turned on to shunt the current of the constant current source, and its drain-source voltage V_{DS1} is;

$$V_{DS1} = V_{in} \tag{26}$$

Equation (26) satisfies $V_{DS} \geq V_{GS} - V_T$, so M_1 works in the saturation region and the gate-source voltage V_{GS1} determines the drain-source current I_{DS1} flowing through M_1. At this time, the current I_{DS1} satisfies;

$$I_{DS1} = B_o(V_{GS1} - V_T)^2(1 + \lambda V_{DS1}) \tag{27}$$

The rise of V_{in} will cause V_{GS1} to rise, and a small change of V_{GS1} will cause a larger change of I_{DS1}. When the drain-source current I_{DS2} of M_2 and I_{DS1} satisfies the following relationship, the circuit keeps a new steady state.

$$I_{DS1} + I_{DS2} = I_{in} \tag{28}$$

In this steady state, the load current is still equal to the current flowing through M_2. As analyzed in Section 2.2, V_{DS2} no longer satisfies the condition of $V_{DS} = V_{GS} - V_T$. The M_2 works in the unsaturation region and $V_{DS2} \ll V_{in}$.

$$I_{load} = I_{DS2} = \frac{V_{in} - V_{DS2}}{R_{load}} \approx \frac{V_{in}}{R_{load}} \tag{29}$$

According to $V_{GS1} = V_{in} - V_{Z1}$, the change of V_{GS1} is equal to V_{in}. In addition, the maximum and minimum values of V_{GS1} and V_{in} are obtained at the same time. In (27), V_T and B_0 are both fixed values which are only related to the properties of the MOSFETs, and $V_{DS1} = V_{in}$. So the minimum value of I_{DS1} is obtained when V_{GS1} and V_{in} are the minimum value, and the maximum value of I_{DS1} is obtained when V_{GS1} and V_{in} are the maximum value.

When $R_{load} = R_{E1}$, $I_{DS2} \approx I_{in}$. MOSFET M_1 is critical turned on and $I_{DS1} \approx 0$. Substituting $I_{DS1} \approx 0$ into (27), we can obtain;

$$V_{GS1MIN} = V_T \tag{30}$$

When $R_{load} = \infty$, $I_{DS2} \approx 0$, I_{DS1} is at maximum, and $I_{DS1} = I_{in}$. Substituting $I_{DS1} = I_{in}$ into (27), we can obtain;

$$V_{GS1MAX} = \sqrt{\frac{I_{in}}{B_0(1 + \lambda V_{in})}} + V_T \tag{31}$$

where, $1 + \lambda V_{in} > 1$. We can determine the change of V_{GS1} from (30) and (31);

$$\Delta V_{GS1} = \sqrt{\frac{I_{in}}{B_0(1 + \lambda V_{in})}} < \sqrt{\frac{I_{in}}{B_0}} \tag{32}$$

Similarly, assuming that the output current of the constant current source is 1A and $B_0 \approx 1$, the change of V_{GS1} is $\Delta V_{GS1} < 1V$, therefore $V_{GS1} \approx V_T$. When the load changes between R_{E1} and ∞ (including an open circuit fault of the load, i.e. $R_{load} = \infty$), $\Delta V_{in} < 1V$ because $\Delta V_{GS1} = \Delta V_{in}$.

The output voltage of the constant current source in this steady state is;

$$V_{in} = V_{Z1} + V_{GS1} \approx V_{Z1} + V_T \quad (33)$$

The load can be equivalently powered by a constant voltage source in this steady state and the voltage of the load is;

$$V_{load} = V_{in} - V_{DS2} \approx V_{in} \quad (34)$$

When $R_{load} \in [R_{E1}, \infty]$, for the constant current source, the equivalent load resistance R_{eq} of this control circuit and load is;

$$R_{eq} = R_{E1} \quad (35)$$

The power consumption of M_2 is $P_{M2} = V_{DS2}I_{in}$, and V_{DS2} is usually less than 1V. Assuming $I_{in} = 1A$, we can obtain $P_{M2} < 1W$.

The power consumption of M_1 in this steady state is;

$$P_{M1} = V_{DS1}I_{DS1} = V_{in}(I_{in} - \frac{V_{in}}{R_{load}}) \quad (36)$$

Since $V_{in}I_{in}$ is approximately a fixed value, the power consumption of M_1 increases with the increase of load resistance. In extreme cases, when $R_{load} = \infty$, $I_{DS1} = I_{in}$. In this scenario, the power consumption of M_1 is the largest and P_{M1MAX} is equal to the input power P_{in}.

In summary,

When $R_{load} \in [0, R_{E2}]$, the load of the power control circuit is equivalently powered by the constant current source and $I_{load} = I_{in}$, the output voltage of the constant current source is $V_{in} = V_{Z2} + V_{GS2} \approx V_{Z2} + V_T$;

When $R_{load} \in (R_{E2}, R_{E1})$, the load of the power control circuit is equivalently powered by the constant current source, and $I_{load} = I_{in}$, the output voltage of the constant current source is $V_{in} \approx I_{in}R_{load}$ with a voltage change of $\Delta V_{in} = V_{Z1} - V_{Z2}$;

When $R_{load} \in [R_{E1}, \infty]$, the load of the power control circuit is equivalently powered by the constant voltage source, and $V_{load} = V_{in} - V_{DS2} \approx V_{in}$, the output voltage of the constant current source is $V_{in} = V_{Z1} + V_{GS1} \approx V_{Z1} + V_T$.

The circuit changes the working state of M_1 and M_2 according to the change of the load. When $R_{load} \geq R_{E1}$(including when the load has an open circuit fault), M_1 will bear the excess power of the constant current source generated by the load change. However, when $R_{load} \leq R_{E2}$(including when the load has a short circuit fault), M_2 will bear the excess power of the constant current source. The equivalent load is basically unchanged or is changed within a very small range for the constant current source, the equivalent load $R_{eq} \in (R_{E2}, R_{E1})$, which allows the constant current source to maintain stable output voltage and output power and improves the reliability of the underwater power supply system. The output voltage of the constant current source is $V_{in} \in (V_{Z2} + V_T, V_{Z1} + V_T)$. The change of V_{in} is $\Delta V_{in} = V_{Z1} - V_{Z2}$, and is determined by the voltage regulation value of the zener diodes.

IV. DEFINITION OF THE RATED LOAD AND SELECTION METHOD FOR THE MAIN COMPONENT PARAMETERS

A. RATED LOAD R_e

Under the condition of a given constant current source, the rated load is the maximum effective load, which should meet the following requirements: (1) When $R_{load} \leq R_e$, the output current of the circuit remains constant and is equal to the output current of the constant current source; (2) When $R_{load} = R_e$, the insertion loss of the circuit is minimal.

B. SELECTION METHOD OF MAIN COMPONENT PARAMETERS

1) ZENER DIODES

The difference $V_{Z1} - V_{Z2}$ of regulated voltage value between Z_1 and Z_2 reflects the output voltage change of the constant current source when the load resistance changes within a large range. In order to reduce the requirements for components, generally we make V_{Z1} larger than V_{Z2} by 3~5V. V_{Z1} and V_{Z2} are determined by the value of the rated load, and according to the analysis in Section III, V_{Z1} and V_{Z2} should make R_e satisfy the following relationship,

$$R_{E2} \leq R_e < R_{E1} \quad (37)$$

i.e. V_{Z1} and V_{Z2} should satisfy;

$$V_{Z2} \leq I_{in}R_e - V_T < V_{Z1} \quad (38)$$

Generally, we can make $V_{Z2} = I_{in}R_e - V_T$.

2) CURRENT-LIMITING RESISTORS

In order to limit the current flowing through the zener diodes and ensure that the diodes can work normally, the current-limiting resistors R_1 and R_2 are generally selected to $1k\Omega \sim 10k\Omega$ to ensure that the current in the zener diodes branch is low. It can be ignored compared to the MOSFET branch current.

3) MOSFETS

The MOSFETs M_1 and M_2 need to bear the excess power consumption when the load changes. This power consumption causes the MOSFETs to heat up and the temperature rises. The maximum allowable power dissipation [33] of the MOSFETs can be expressed as;

$$P_{DM} = \frac{T_{JM} - T_C}{R_{JC}} \quad (39)$$

where, T_{JM} is the rated junction temperature of the MOSFET, T_C is the case temperature, R_{JC} is the junction-to-case thermal resistance which characterizes the heat transfer capacity of the medium, and the unit of R_{JC} is °C/W. The P_{DM} given in the device manual is usually the maximum

TABLE 1. Measurement data from simulation.

| R_{load} / Ω	I_{load} / A	V_{load} / V	V_{in} / V
0.01	1.0	0.01	104.24
50	1.0	49.98	104.26
100	1.0	99.96	104.28
104	1.0	103.95	104.43
106	1.0	105.92	106.30
108	1.0	107.84	108.21
110	0.98	108.33	108.69
200	0.54	108.91	109.11
300	0.36	109.02	109.16
10M	0	109.24	109.24

allowable power dissipation when the case temperature is 25°C. The dissipation capacity of the MOSFET is reduced when $T_C > 25°C$. The maximum allowable power dissipation should meet $P_{in} < P_{DM}$ and leave some margin, where $P_{in} = I_{in}^2 R_e$. Also, the maximum withstand voltage $V_{\max}$ should meet $V_{\max} > V_{Z1} + V_T$ and the maximum current $I_{\max}$ should meet $I_{\max} > I_{in}$.

V. VERIFICATION AND ANALYSIS OF THE EQUIVALENT LOAD POWER-STABILITY CONTROL CIRCUIT

A. SIMULATION VERIFICATION AND ANALYSIS

In order to verify the correctness of the theoretical analysis, the circuit shown in Figure 1 was built in the Saber program for simulation verification. The specific design parameters are as follows. MOSFETs M_1 and M_2 are IRF450 and their turn-on voltage V_T is approximately 4V. The constant current source output current I_{in} is 1A. Assuming the rated load R_e is 104Ω, the regulated voltage value V_{Z2} of Z_2 sets to 100V and the regulated voltage value V_{Z1} of Z_1 sets to 105V. The current-limiting resistors R_1 and R_2 are 10$k\Omega$. For IRF450, the rated junction temperature is 150 °C, the junction-to-case thermal resistance is 0.83 °C/w, and the maximum allowable power dissipation is 150W at the case temperature of 25 °C. The output power of the constant current source meets $P_{in} < P_{DM}$ with some margin. Table 1 shows the simulation data for the changes in load resistance.

When the load resistance value continuously changes from 0 to 200Ω, the curves of the output current, output voltage, and constant current source output voltage of the circuit are as shown in Figure 5.
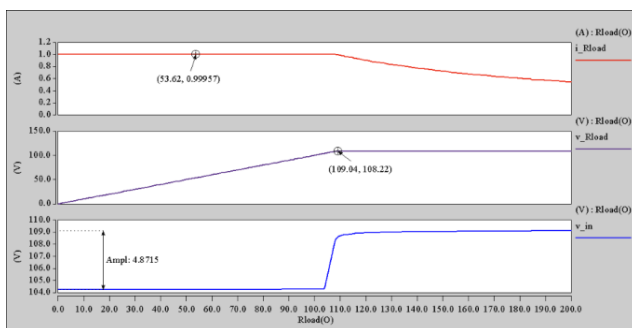
**FIGURE 5.** Simulation curves of input and output characteristics with load resistance continuously changing from 0 to 200 Ω.

Where, i_Rload, v_Rload and v_in are load current I_{load}, load voltage V_{load} and output voltage V_{in} of constant current source respectively.

Consideration of Figure 4 and Table 1 reveals that when $R_{load} \leq R_e$ (including when the load has a short circuit fault), the load current I_{load} is kept constant at 1A and the voltage V_{in} is maintained at about 104V, which is consistent with the theoretical value $V_{Z2} + V_T = 100V + 4V = 104V$. When $R_{load} > R_e$ and M_1 is not yet turned on, the voltage V_{in} increases as the load increases. When $R_{load} > R_e$ and M_1 is turned on (including when the load has an open circuit fault), the voltage V_{in} and V_{load} are maintained at about 109V, consistent with the theoretical value $V_{Z1} + V_T = 105V + 4V = 109V$. In addition, the current I_{load} is reduced because the output current of the constant current source I_{in} is shunted by M_1.

When the change of load is 0.01 -10MΩ (including when the load has an open circuit or short circuit fault), the change of constant current source output voltage is 5V, which is consistent with the theoretical value $\Delta V_{in} = V_{Z1} - V_{Z2} = 105V - 100V = 5V$. The simulation results are highly consistent with the theoretical analysis. When $R_{load} = 104\Omega = R_e$, the load power is 103.95W while the output power of the constant current source is 104.43W, the insertion loss is 0.48W, and the transmission efficiency is 99.5%.

B. EXPERIMENTAL VERIFICATION AND ANALYSIS

In the theoretical analysis, when $R_{load} \in [0, R_{E2}]$ or $R_{load} \in [R_{E1}, \infty]$, the change of the constant current source output voltage is less than $\sqrt{I_{in}/B_0}$ (B_0 is related to the properties of the MOSFETs). According to (4), there is a functional relationship between I_{DS}, B_0, V_{GS}, and V_{DS}. In order to obtain the B_0 of the IRF450 used in this experiment, the V_{DS} was set to 10V and 20V in turn while changing the value of V_{GS}. The current I_{DS} was measured, and then the data fitting was performed with MATLAB. The experimental and fitting results are shown in Figure 6.
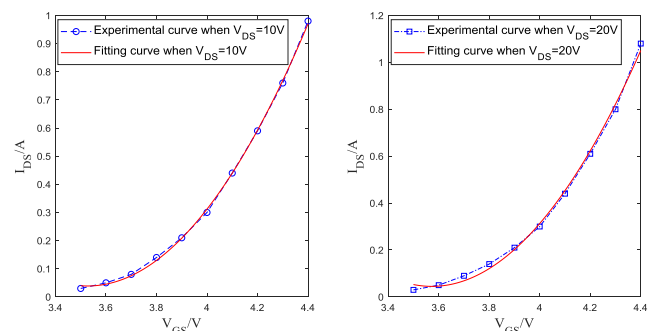
FIGURE 6. Experimental and fitting curves of MOSFET transfer characteristics.

According to the fitting results, we can obtain $V_T = 3.55V$, $\lambda = 0.025$, $B_0 = 0.98$, which verifies the assumptions in the theoretical analysis.

TABLE 2. Measurement data from experiment.

R_{load} / Ω	I_{load} / A	V_{load} / V	V_{in} / V
0.3	0.498	0.016	106.4
1	0.498	4.9	107
10	0.498	4.98	107
30	0.498	15.2	107
50	0.498	24.9	110.5
100	0.498	49.9	110.8
150	0.496	74.6	111.4
180	0.496	89.4	110.5
190	0.495	94.5	111.5
200	0.495	99.4	111.6
210	0.496	104.29	109.7
220	0.495	109.5	110.2
250	0.496	113.9	115
280	0.412	115.4	115.9
300	0.384	115.57	116.1
500	0.231	115.7	116
1000	0.114	115.3	115.5
2000	0.055	114.9	114.6

In order to further verify the practicability of the equivalent load power control circuit, we built a prototype. The experimental parameters were as follows: MOSFETs M_1 and M_2 were IRF450 with a turn-on voltage V_T of about 4V; the output current of the constant current source I_{in} was 0.5A. Assuming the rated load R_e of the circuit to be 220Ω, the regulated voltage value V_{Z2} of Z_2 was set to 102V and the regulated voltage value V_{Z1} of Z_1 was set to 107V. The current-limiting resistors R_1 and R_2 were 1$k\Omega$. According to the previous theoretical analysis, the output power of the constant current source met the relationship of $P_{in} \approx I_{in}(V_{Z1} + V_T) = 55.5W < P_{DM}$ with some margin. The experimental data is shown in Table 2.

The curves of the output current, output voltage, and constant current source output voltage with load resistance changes are shown in Figure 7.
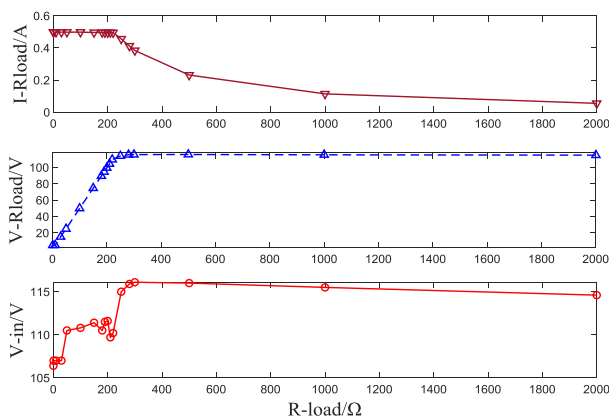

FIGURE 7. Experimental curves of input and output characteristics with load resistance changes from 0 to 2000 Ω.

Where, I_Rload, V_Rload and V_in are load current I_{load}, load voltage V_{load} and output voltage V_{in} of constant current source respectively.

When $R_{load} \leq R_e$, the average of the load current I_{load} was 0.497A, and the error between I_{load} and theoretical output current 0.5A was 6‰. The average of the voltage V_{in} was 109.4V, the theoretical value is $V_{Z2} + V_T = 106V$, and the error between V_{in} and theoretical value was 3.2‰. When $R_{load} > R_e$ and M_1 was not yet turned on, the voltage V_{in} increased as the load increased. When $R_{load} > R_e$ and M_1 was turned on, the average of the voltage V_{load} was 114.32V and the average of the voltage V_{in} was 114.76V. The theoretical values of V_{load} and V_{in} are $V_{Z1} + V_T = 111V$, and the error of V_{load} was 2.99% while the error of V_{in} was 3.39%.

In the wide range of load resistance from 0.3 to 2000Ω, the average change of V_{in} was 5.36V, which was 7.2% higher from the theoretical value $\Delta V_{in} = V_{Z1} - V_{Z2} = 5V$. The difference between the maximum and the minimum values of V_{in} was 9.7V. The experimental results verify the correctness of the theoretical analysis. When $R_{load} = 220\Omega = R_e$, the load power was 54.20W while the output power of the constant current source was 55.1W, the insertion loss was 0.9W, and the transmission efficiency was 98.37%. The experimental results are not as close to the theoretical values as the simulation results, because in practice there will be slight fluctuations in the regulated voltage value of zener diodes and the turn-on voltage of MOSFETs.

In our prototype system of CUINs, there were 3 events where the voltage at the node increased rapidly and exceeded the withstand voltage value of the component due to an open-circuit fault at the load. The reasons were wrong operation, damaged submarine cable ground wire and faulty module. Even more, these caused the device to burn out and all electrical equipment connected to the node to fail. The device before and after burning is shown in Figure 8.
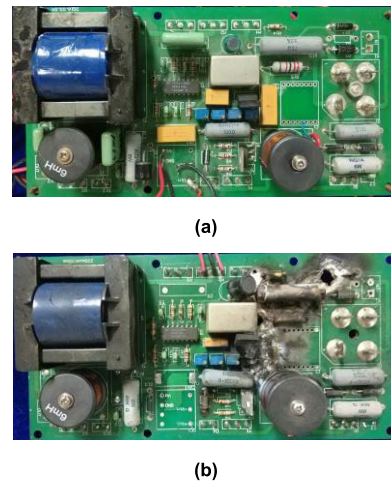

FIGURE 8. Display diagram of device before and after burning: (a) Diagram of device before burning; (b) Diagram of device after burning.

In order to avoid the influence on circuit due to fault at the load, the overvoltage or overcurrent protection is generally adopted, and the control switch is used to cut off the power supply of the faulty part. This strategy can only protect the damaged module from further destruction, and

cannot ensure the stability of the power supply system. For this reason, we designed a control circuit and connected it in series between the constant current power supply and the load in order to reduce the impact of load changes on the power supply system. Experimental results show that, with the same change of load, the addition of this control circuit can effectively reduce output voltage fluctuation of the constant current source.

In summary, when $R_{load} \leq R_e$, the load on the circuit is equivalent to what it would be if powered by a constant current source I_{in}. When $R_{load} > R_e$ and M_1 is turned on, the load is equivalent to what it would be if powered by a constant voltage source $V_{Z1} + V_T$. When the load resistance changed within a wide range, the output voltage of the constant current source satisfies $V_{in} \in (V_{Z2} + V_T, V_{Z1} + V_T)$ and the range of change is $\Delta V_{in} = V_{Z1} - V_{Z2}$. The results show that the addition of this control circuit can effectively reduce output voltage fluctuation of the constant current source. The equivalent load for the constant current source is basically unchanged or is changed within a very small range (determined by the difference between the regulated voltage values of the two zener diodes). This keeps the constant current source output power stable and improves reliability of the constant current remote power supply system for CUINs.

VI. CONCLUSION

We propose a novel equivalent load power-stability control circuit aimed at improving stability of the constant current remote power supply system for CUINs. After theoretical analysis, simulation, and experimental verification, we found that the equivalent load power-stability control circuit design can enable MOSFETs to change their own working state according to the change of load and play a role in power compensation. When load resistance changes within a large range (including when the load has an open circuit or short circuit fault), the equivalent load is basically unchanged or is changed within a very small range for the constant current source, which keeps the constant current source output voltage and output power stable. When the load resistance of the circuit is the rated load, transmission efficiency is greater than 98%. The design has strong practicability because it can reduce the influence of the branch line cable on the trunk line cable and can improve the reliability of the underwater constant current remote power supply system as a whole. Furthermore, the design is conducive to standardization and serialization of CUINs and opens up the possibility of live equipment replacement and maintenance for CUINs. The disadvantage of this design is that when the load changes within a wide range, the MOSFETs may need to bear larger power consumption.

REFERENCES

[1] Y. Chen, *Fundamentals of Ocean Technology*. Beijing, China: Ocean Press, 2018, pp. 227–235.

[2] F. Lu, H. Zhou, X. Peng, J. Yue, and P. Wang, "Technical preparation and prototype development for long-term cabled seafloor observatories in Chinese marginal seas," in *Seafloor Observatories*. Berlin, Germany: Springer, 2015, ch. 19, pp. 503–529.

[3] L. Carter, "Environmental impacts," in *Submarine Cables Oceans: Connecting World*. London, U.K.: Lavenham Press, 2009, ch. 5, pp. 29–37.

[4] F. Lü and H. Zhou, "Progress of scientific cabled seafloor observatory networks," *J. Eng. Stud.*, vol. 8, pp. 139–154, Feb. 2016.

[5] Z. Gao and G. Guo, "Fixed-time leader-follower formation control of autonomous underwater vehicles with event-triggered intermittent communications," *IEEE Access*, vol. 6, pp. 27902–27911, 2018.

[6] R. Diamant and L. Lampe, "Low probability of detection for underwater acoustic communication: A review," *IEEE Access*, vol. 6, pp. 19099–19112, 2018.

[7] C. Hua, "Technologies of cabled submarine networking observation," in *International Progress in Submarine Scientific Observation*. Shanghai, China: Tongji Univ. Press, 2017, ch. 9, pp. 139–154.

[8] J. Chesnoy, "Terminal equipment," in *Undersea Fiber Communication Systems*, 2nd ed. Cambridge, MA, USA: Academic, 2016, ch. 10, pp. 237–260.

[9] W. Pinxian, "Seafloor observatories: The third platform for Earth system observation," *Chin. J. Nature*, vol. 29, no. 3, pp. 125–130, Jul. 2007.

[10] L. D. Garrett, "Design of global submarine networks [Invited]," *J. Opt. Commun. Netw.*, vol. 10, no. 2, p. A185, Feb. 2018.

[11] Z. Zhang, X. Zhou, X. Wang, and L. Wang, "A novel diagnosis and location method of short-circuit grounding high-impedance fault for a mesh topology constant current remote power supply system in cabled underwater information networks," *IEEE Access*, vol. 7, pp. 121457–121471, 2019.

[12] Y. Chen, B. M. Howe, and C. Yang, "Actively controllable switching for tree topology seafloor observation networks," *IEEE J. Ocean. Eng.*, vol. 40, no. 4, pp. 993–1002, Oct. 2015.

[13] M. A. El-Sharkawi, A. Upadhye, S. Lu, H. Kirkham, B. M. Howe, T. McGinnis, and P. Lancaster, "North east pacific time-integrated undersea networked experiments (NEPTUNE): Cable switching and protection," *IEEE J. Ocean. Eng.*, vol. 30, no. 1, pp. 232–240, Jan. 2005.

[14] C. R. Barnes, M. M. R. Best, F. R. Johnson, L. Pautet, and B. Pirenne, "Challenges, benefits, and opportunities in installing and operating cabled ocean observatories: Perspectives from NEPTUNE Canada," *IEEE J. Ocean. Eng.*, vol. 38, no. 1, pp. 144–157, Jan. 2013.

[15] S. Monna, G. Falcone, L. Beranzoli, F. Chierici, G. Cianchini, M. De Caro, A. De Santis, D. Embriaco, F. Frugoni, G. Marinaro, C. Montuori, L. Pignagnoli, E. Qamili, T. Sgroi, and P. Favali, "Underwater geophysical monitoring for European multidisciplinary seafloor and water column observatories," *J. Mar. Syst.*, vol. 130, pp. 12–30, Feb. 2014.

[16] Y.-H. Chen, C.-J. Yang, D.-J. Li, B. Jin, and Y. Chen, "Study on 10 kVDC powered junction box for a cabled ocean observatory system," *China Ocean Eng.*, vol. 27, no. 2, pp. 265–275, Apr. 2013.

[17] X. Zhou, C. Fan, D. Li, and Y. Zhou, "Power scheme selecting method for constant current power system of cabled seafloor observatory network," *Autom. Electr. Power Syst.*, vol. 39, no. 19, pp. 126–131, Oct. 2015.

[18] J.-K. Choi, S. Nishida, T. Yokobiki, and K. Kawaguchi, "Automated cable-laying system for thin optical-fiber submarine cable installation," *IEEE J. Ocean. Eng.*, vol. 40, no. 4, pp. 981–992, Oct. 2015.

[19] J.-K. Choi, T. Yokobiki, and K. Kawaguchi, "ROV-based automated cable-laying system: Application to DONET2 installation," *IEEE J. Ocean. Eng.*, vol. 43, no. 3, pp. 665–676, Jul. 2018.

[20] A. Aboulian, D. H. Green, J. F. Switzer, T. J. Kane, G. V. Bredariol, P. Lindahl, J. S. Donnal, and S. B. Leeb, "NILM dashboard: A power system monitor for electromechanical equipment diagnostics," *IEEE Trans. Ind. Informat.*, vol. 15, no. 3, pp. 1405–1414, Mar. 2019.

[21] F. Zhang, B. Jin, D. Li, Y. Chen, C. Yang, and H. Yang, "Study on the short fault isolation of cabled ocean observatory," in *Proc. OCEANS MTS/IEEE Monterey*, Monterey, CA, USA, Sep. 2016, pp. 1–5.

[22] Z. Zhang, X. Zhou, X. Wang, and T. Wu, "Design, analysis, and modeling of an isolated constant-current to constant-voltage converter in cabled underwater information networks," *Electronics*, vol. 8, no. 9, p. 961, Aug. 2019.

[23] D. W. Harris and F. K. Duennebier, "Powering cabled ocean-bottom observatories," *IEEE J. Ocean. Eng.*, vol. 27, no. 2, pp. 202–211, Apr. 2002.

[24] R. A. Petitt, D. W. Harris, B. Wooding, J. Bailey, J. Jolly, E. Hobart, A. D. Chave, F. Duennebier, R. Butler, A. Bowen, and D. Yoerger, "The Hawaii-2 observatory," *IEEE J. Ocean. Eng.*, vol. 27, no. 2, pp. 245–253, Apr. 2002.

[25] B. M. Howe, R. Lukas, F. Duennebier, and D. Karl, "ALOHA cabled observatory installation," in *Proc. OCEANS MTS/IEEE KONA*, Waikoloa, HI, USA, Sep. 2011, pp. 1–11.

[26] J. Kasahara, R. Iwase, T. Nakatsuka, Y. Nagaya, Y. Shirasaki, K. Kawaguchi, and J. I. Kojima, "An experimental multi-disciplinary observatory (VENUS) at the ryukyu trench using the Guam-Okinawa geophysical submarine cable," *Ann. Geophys.*, vol. 49, no. 2, pp. 595–606, Apr. 2006.

[27] K. Kawaguchi, E. Araki, Y. Kogure, N. Takahashi, T. Katayama, K. Hishiki, N. Fujiwara, N. Iida, and Y. Kaneda, "Development of DONET2-Off Kii chanel observatory network," in *Proc. IEEE Int. Underwater Technol. Symp. (UT)*, Tokyo, Japan, Mar. 2013, pp. 1–5.

[28] T. Yokobiki, J.-K. Choi, S. Nishida, H. Matsumoto, E. Araki, K. Kawaguchi, N. Takahashi, and S. Kodaira, "Construction of DONET2," in *Proc. Techno-Ocean (Techno-Ocean)*, Kobe, Japan, 2016, pp. 435–438.

[29] Y.-H. Chen, S. Xiao, and D.-J. Li, "Power system design for constant current subsea observatories," *Frontiers Inf. Technol. Electron. Eng.*, vol. 20, no. 11, pp. 1505–1515, Nov. 2019.

[30] K. Takehira, "Submarine system powering," in *Undersea Fiber Communication Systems*, 2nd ed. Cambridge, MA, USA: Academic, 2016, ch. 10, pp. 381–402.

[31] Y. Chen, Y. Zang, C. Yang, Z. Duan, H. Zhang, and G. Muhammad, "Reconfigurable power converter for constant current underwater observatory," *Electronics*, vol. 9, no. 2, p. 307, Feb. 2020.

[32] J. Kojima, B. M. Howe, K. Asakawa, and H. Kirkham, "Power systems for ocean regional cabled observatories," in *Proc. Oceans MTS/IEEE Techno-Ocean*, Kobe, Japan, Nov. 2004, pp. 2176–2181.

[33] S. Tong and C. Hua, *Basics of Analog Electronics*. Beijing, China: Higher Education, 2015, pp. 39–50.

LEI WANG received the B.Eng. degree from the Ocean University of China (OUC), Qingdao, China, in 2018. He is currently pursuing the M.Eng. degree with the Naval University of Engineering (NUE), Wuhan, China.

Since 2018, he has been participating in the Natural Science Foundation of Hubei Province, China, the power supply laboratory prototype system construction of the cabled underwater information network. His research interests include fiber optics, underwater cabled optical communication, and underwater remote power supply systems.

XUEJUN ZHOU was born in Wuwei, Gansu, China, in 1962. He received the B.Eng. degree from Xidian University, Xi'an, China, in 1984, the M.Eng. degree in communication and electronic system from the PLA University of Science and Technology, Nanjing, China, in 1988, and the Ph.D. degree in communication engineering from the National University of Defense Technology, Changsha, China, in 2003.

From 1996 to 2001, he was an Associate Professor with the Naval College of Electronic Engineering. Since 2002, he has been a Professor with the College of Electronic Engineering, Naval University of Engineering (NUE). He has been the Chief Professor with the Department of Information Network Engineering, NUE, since 2015. He is the author of two books and more than 110 articles. He holds four patents. His research interests include underwater cabled optical communication, quantum secure communication, and underwater remote power supply systems.

ZHENG ZHANG received the B.Eng. degree from Hohai University (HHU), Nanjing, China, in 2014, and the M.Eng. and Ph.D. degrees in communication and information system from the Naval University of Engineering (NUE), Wuhan, China, in 2016 and 2019, respectively.

Since 2019, he has been an Engineer with the Unit 75842, Chinese People's Liberation Army. Since 2015, he has been participating in the Natural Science Foundation of Hubei Province, China, the National Natural Science Foundation of China (NSFC), and military research projects for many times, and completed the deep sea test of the constant current remote supply system equipment, and the power supply laboratory prototype system construction of the cabled underwater information network. His research interests include fiber optics, underwater cabled optical communication, and underwater remote power supply systems.

• • •